SIMPLIFICATION OF THE DYNAMIC MODEL OF A HYDRAULIC ROCKBREAKER FOR THE PURPOSE OF IMPLEMENTATION IN A MODEL-BASED CONTROL SCHEME

Louis-Francis Y. Tremblay, Marc Arsenault, Meysar Zeinali
Bharti School of Engineering, Laurentian University, Sudbury, ON, CA
Email: lx2_tremblay@laurentian.ca; marsenault@laurentian.ca; mzeinali@laurentian.ca

ABSTRACT

Research in the automation of hydraulic excavators and rockbreakers is becoming more and more prominent. A model-based approach to control such machines necessitates an adequate dynamic model in order to increase the robustness of the controller and improve its performance (e.g., reduce tracking error). Most previous efforts in the development of dynamic models for excavators have made the assumption of planar motion while also neglecting the dynamic effects due to the presence of hydraulically-driven prismatic actuators. In this paper, the dynamic model of the mechanical subsystem of a hydraulic rockbreaker is developed using the Euler-Lagrange formulation. The model considers the contributions of the hydraulic actuators and does not assume planar motion. Potential simplifications to the dynamic model are then introduced with the objective of facilitating the model's parameterization for the purpose of developing an adaptive control algorithm. In order to evaluate their level of accuracy, these simplified dynamic models are then evaluated based on the required joint torques for specified trajectories. It is shown that the proposed simplifications reduce the complexity of the dynamic model while preserving its accuracy and simplicity which is attractive for real-time control applications.

Keywords: hydraulic rockbreaker; dynamic modeling; automation.

SIMPLIFICATION DU MODÈLE DYNAMIQUE D'UN BRISE-ROCHE HYDRAULIQUE POUR PERMETTRE SON UTILISATION DANS UN ALGORITHME DE COMMANDE À BASE D'UN MODÈLE DYNAMIQUE

RÉSUMÉ

Le développement d'excavatrices et de brises-roches hydrauliques automatisés a fait l'objet de plusieurs recherches récentes. La commande de tels systèmes à partir d'algorithmes fondés sur des modèles dynamiques nécessite que ces modèles soient suffisamment détaillés pour assurer une performance adéquate. Dans la plupart des travaux existants portant sur la modélisation dynamique d'excavatrices, les mouvements de ces dernières sont limités à un plan tandis que les contributions de leurs vérins hydrauliques sur le modèle dynamique sont négligées. Dans cet article, le modèle dynamique des composants mécaniques d'un brise-roche hydraulique est développé à partir de la formulation de Euler-Lagrange. Le modèle prend en considération les contributions des vérins hydrauliques et permet les mouvements spatiaux. Des simplifications potentielles pouvant être apportées au modèle sont introduites avec l'objectif de faciliter la paramétrisation du modèle pour permettre son utilisation dans un algorithme de commande adaptatif. Pour évaluer la performance des modèles dynamiques simplifiés, ces derniers sont évalués en fonction des couples correspondants devant être fournis aux articulations rotoïdes pour des trajectoires spécifiées. Il est démontré que les contributions des vérins hydrauliques au modèle dynamique du brise-roche sont, dans plusieurs cas, négligeables.

Mots-clés : brises-roches hydrauliques ; modélisation dynamique ; automatisation.

1. INTRODUCTION

A rockbreaker is a hydraulically actuated machine commonly used in the mining and construction industries to fracture large pieces of material into smaller pieces that are sifted through a metal grid known as a grizzly. With advancements in the field of robotics, interest in the automation of such systems, along with hydraulic excavators, has grown. In order to achieve suitable control of such devices, nonlinear control algorithms are typically designed with compensators and/or are based on the system's behaviour during operation as described by its dynamic model. Due to the presence of complex phenomena such as joint friction, parametric uncertainties and the non-linearity of the hydraulic and mechanical subsystems, the modeling and design of model-based controllers for such systems is difficult and challenging task. Parameter uncertainties may lead to poor system response (e.g., higher trajectory tracking error) during the system's motion. However, such negative effects can be reduced through the use of a robust controller as seen in [1] or adaptive controllers such as the ones presented in [2, 3], which utilize the system's dynamic model in a parameterized form to estimate the approximately known or uncertain parameters of the dynamic model. Therein lies the importance of developing an accurate yet not overly complex dynamic model such that it may be parameterized. There have been numerous papers describing the dynamic modeling of hydraulic excavators in the past, notably following the Newton-Euler conventions [4–6], using Kane's equations [7] or using the Lagrange-Euler convention [8]. All dynamic models presented in [4–8] represent a hydraulic excavator as a planar three-degree-of-freedom (3-DoF) manipulator (where the swing joint of the excavator is not considered). They also neglect the dynamic effects of the hydraulic actuators on the dynamic model . The resulting dynamic models describe the complex link dynamics of an excavator without any simplifications, with the exception of the model presented in [4], which assumes the centre of mass for each link to be in-line with each link's corresponding axis.

While previous works have consistently used simplified dynamic models of large hydraulic machinery, to the authors' knowledge none have validated such simplifications through dynamic simulations. The research presented in this paper seeks to mitigate this shortcoming by developing a detailed dynamic model of a 4-DoF rockbreaker. The scope of the work presented herein includes the rockbreaker mechanism (i.e., links, joints and actuators) but excludes the hydraulic system used for the actuation. The rockbreaker that is considered is assumed to be anchored to a stationary pedestal while interactions with its environment are not considered (the rock breaking operation is outside the scope of this research). In order to reduce the complexity of the dynamic model and ease the implementation of an adaptive control algorithm, the neglect of some terms within the dynamic model will be explored and the corresponding effects will be quantified. The possibility of neglecting terms within the dynamic model is cited by [9], who states that the effects of the Coriolis and centrifugal terms of the dynamic model of excavators are negligible due to the system's relatively low velocities. The goal is to identify a simplified dynamic model of a rockbreaker that represents the actual system with sufficient accuracy while allowing for an easier parameterization to be used in an adaptive controller, similar to the one presented in [2]. It is expected that this would lead to corresponding reductions to the time required within a real-time control algorithm for the computation of the dynamic model although this is not validated in this paper.

2. DESCRIPTION OF ROCKBREAKER SYSTEM

A CAD model of a rockbreaker can be seen in Fig. 1 where the swing post, the inner boom, the outer boom and the breaker have been identified. For the purpose of modeling and analysis, these parts within the rockbreaker may be considered as the links of a four-degree-of-freedom serial robot as represented schematically in Fig. 2 where revolute joints connecting the links are labeled as R_i ($i = 1,2,3,4$). The i^{th} link length, defined as the distance between the axes of revolute joints R_i and R_{i+1}, is represented as a_i (note

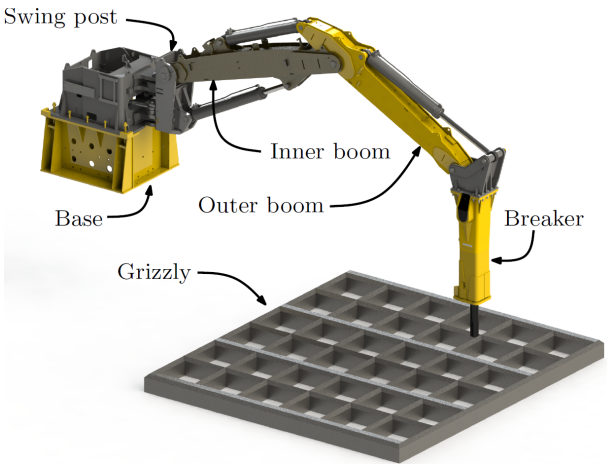

Fig. 1. Typical rockbreaker with grizzly used in underground mining operations.

that reference point P', located at the tip of the breaker, acts in lieu of the non-existent R_5). Meanwhile, the angles of the revolute joints are denoted as θ_i. The rockbreaker's passive revolute joints are actuated indirectly through a series of hydraulically-driven prismatic actuators whose lengths are represented as ρ_j ($j = 0, 1, ..., 4$). This actuation scheme allows for high torques to be efficiently produced at each revolute joint but results in nonlinear relationships between the actuator lengths (ρ_j) and the revolute joint angles (θ_i). It should be noted that revolute joint R_1 is controlled by two actuators (ρ_0 and ρ_1) connected in parallel in order to provide it with a symmetrical torque v. angular displacement curve (see Fig. 2(a)). The actuator lengths ρ_j act as the inputs to the system (through actuation of the hydraulic valves) while the outputs correspond to the combination of the resulting position and orientation of the end-effector. The end-effector's position is described as the location of a reference point P on the breaker that, as shown in Fig. 2(b), is measured from the $X_1Y_1Z_1$ reference frame and is represented as $\mathbf{p} = [x, y, z]^T$. The end-effector's orientation, for its part, is represented by the angle ϕ measured between the X_2 axis and a line joining points P' and P. The centres of mass of the links as well as those of each hydraulic actuator barrel and piston assembly are labeled as C_{l_i}, C_{b_i} and C_{p_i}, respectively. It should be noted that, although they may appear in-line with the prismatic actuators' axes (defined as the lines joining nodes A_i and B_i) in Fig. 2, the centres of mass of the actuator barrels and piston assemblies are generally offset from these axes which adds some complexity to the dynamic model.

To generate the results presented herein, the geometric parameters and inertial properties of all the rigid bodies seen in Fig. 2 were obtained from the CAD model of an existing commercial rockbreaker combined with information extracted from hydraulic actuator data sheets. Tolerances in the manufacturing process, variations in the physical properties of materials and unmodeled effects combine such that the resulting dynamic model is expected to deviate from the actual system. While such deviations could lead to poor performance of the model-based control algorithm, this may be mitigated by the use of an adaptive controller, which would ensure parameter estimates converge toward optimal values.

3. KINEMATIC ANALYSIS

In order to develop the dynamic model of the rockbreaker, knowledge of the rigid bodies' centre of mass positions and velocities as well as the angular velocities of the rigid bodies are required. The system's kinematics are modeled using the Denavit-Hartenberg convention as described in [10] . Based on this convention, reference frames have been defined as seen in Fig. 2 where the i^{th} frame is attached to the $(i-1)^{\text{th}}$ link with origin at R_i (with the exception of frame $X_5Y_5Z_5$ which has its origin at P'). The link offset

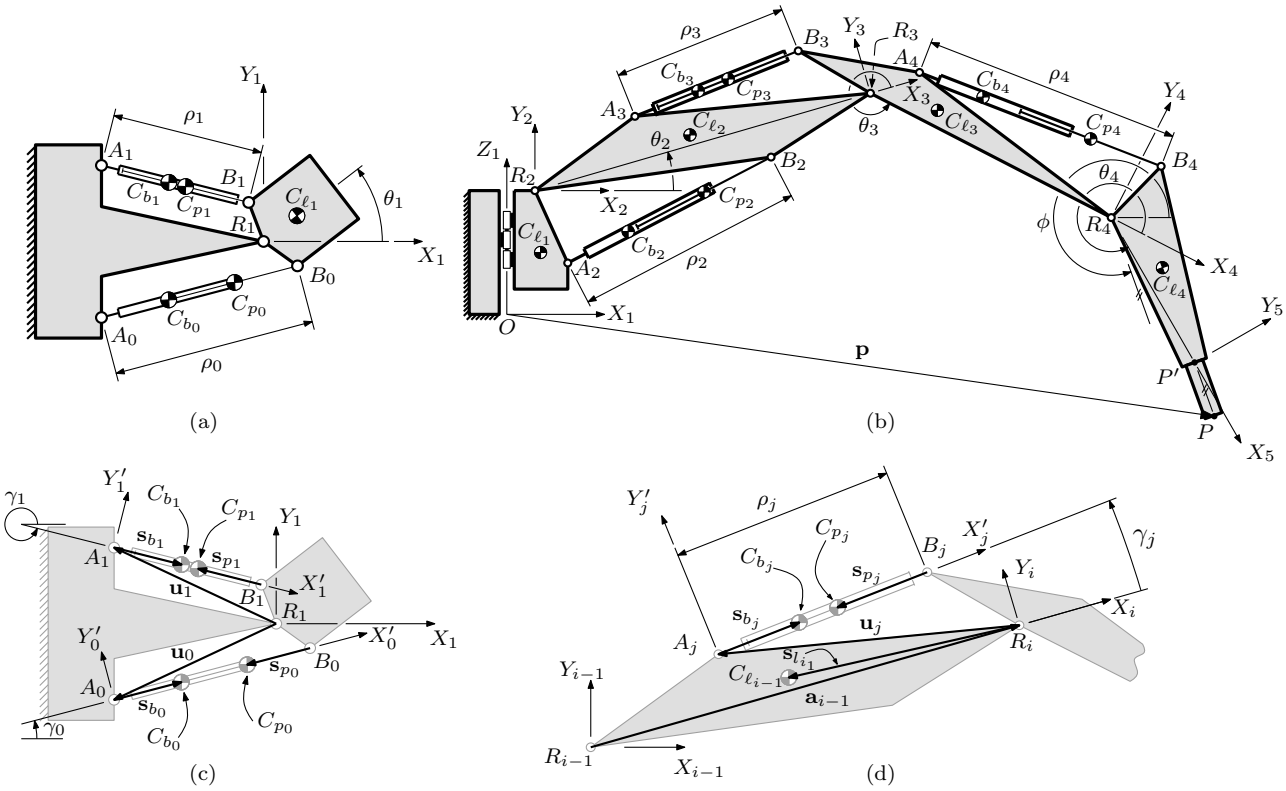

Fig. 2. Schematic representation of rockbreaker with parameter definitions: (a) and (c) Top view of base and swing post, (b) and (d) side view of complete rockbreaker.

is defined as b_i while the link twist is labeled as α_i.The position of the $(i+1)^{\text{th}}$ frame relative to the i^{th} frame is obtained as:

$$[\mathbf{a}_i]_i = [a_i \cos\theta_i, a_i \sin\theta_i, b_i]^T \tag{1}$$

where $[\cdot]_i$ represents a vector expressed in the i^{th} reference frame. Meanwhile, the rotation matrix which rotates the i^{th} frame into the $(i+1)^{\text{th}}$ frame is computed as:

$$\mathbf{Q}_{i+1}^{i} = \begin{bmatrix} \cos\theta_i & -\sin\theta_i \cos\alpha_i & \sin\theta_i \sin\alpha_i \\ \sin\theta_i & \cos\theta_i \cos\alpha_i & -\cos\theta_i \sin\alpha_i \\ 0 & \sin\alpha_i & \cos\alpha_i \end{bmatrix} \tag{2}$$

The position of the centre of mass of the i^{th} link with respect to the $(i+1)^{\text{th}}$ reference frame (which is attached to this link) is defined by the vector $\mathbf{s}_{l_i}$ (see Fig. 2(d)). The position of the centre of mass of the n^{th} link ($n = 1,2,3,4$) with respect to the origin of the $X_1Y_1Z_1$ reference frame may thus be described as:

$$[\bar{\mathbf{c}}_{l_n}]_1 = \sum_{i=1}^{n} [\mathbf{a}_i]_1 + [\mathbf{s}_{l_n}]_1 = [\mathbf{a}_1]_1 + \mathbf{Q}_2^1[\mathbf{a}_2]_2 + \cdots + \mathbf{Q}_2^1\mathbf{Q}_3^2 \ldots \mathbf{Q}_n^{n-1}[\mathbf{a}_n]_n + \mathbf{Q}_2^1\mathbf{Q}_3^2 \ldots \mathbf{Q}_{n+1}^{n}[\mathbf{s}_{l_n}]_{n+1} \tag{3}$$

As for the absolute angular velocity of the n^{th} link, it may be obtained as:

$$[\boldsymbol{\omega}_{l_n}]_1 = \sum_{i=1}^{n} \mathbf{Q}_i^1 \begin{bmatrix} 0 & 0 & \dot{\theta}_i \end{bmatrix}^T \tag{4}$$

where $\mathbf{Q}_1^1 = \mathbf{1}_{3\times 3}$ is the identity matrix and where $\mathbf{Q}_i^1 = \mathbf{Q}_2^1\mathbf{Q}_3^2 \ldots \mathbf{Q}_i^{i-1}$.

A similar approach is used to define the positions of the centres of mass and the absolute angular velocities of the actuator barrels and piston assemblies. The position of the centre of mass of the j^{th} actuator barrel measured from node A_j is defined as $\mathbf{s}_{b_j}$. Likewise, the position of the centre of mass of the j^{th} actuator piston assembly, measured from node B_j, is defined as $\mathbf{s}_{p_j}$. Both of these vectors are constant in a frame $X'_jY'_jZ'_j$ which is defined as having its X'_j axis directed from A_j to B_j while its Z'_j axis is parallel to the axis of the passive revolute joint at A_j as shown in Fig. 2(c) and (d). The rotation matrix bringing the $X_iY_iZ_i$ frame parallel to the $X'_jY'_jZ'_j$ is:

$$\mathbf{Q}^i_{j'} = \begin{bmatrix} \cos\gamma_j & -\sin\gamma_j & 0 \\ \sin\gamma_j & \cos\gamma_j & 0 \\ 0 & 0 & 1 \end{bmatrix} \tag{5}$$

where γ_j is measured from the X_i axis to the X'_j axis. Finally, vector $\mathbf{u}_j$ is defined as being directed from R_i to A_j where $i = j$ when $j = 1,2,3,4$ and $i = j+1$ when $j = 0$. It is noted that this vector is constant in the $X_iY_iZ_i$ frame. With these definitions, the positions of the centres of mass of the n^{th} actuator barrel and piston assembly, for the case where $n = 0,1$, are obtained as:

$$[\bar{\mathbf{c}}_{b_n}]_1 = [\mathbf{u}_n]_1 + \mathbf{Q}^1_{n'}[\mathbf{s}_{b_n}]_{n'}, \quad [\bar{\mathbf{c}}_{p_n}]_1 = [\mathbf{u}_n]_1 + \mathbf{Q}^1_{n'}\left(\rho_n[\mathbf{i}_{n'}] + [\mathbf{s}_{p_n}]_{n'}\right) \tag{6}$$

where $\mathbf{i}_{j'}$ is a unit vector directed along the X'_j axis. Similarly, the positions of the centres of mass of the n^{th} actuator barrel and piston assembly, for cases where $n = 2,3,4$, may be found as:

$$\begin{aligned} [\bar{\mathbf{c}}_{b_n}]_1 &= \sum_{j=1}^{n-1}[\mathbf{a}_j]_1 + [\mathbf{u}_n]_1 + [\mathbf{s}_{b_n}]_1 \\ &= [\mathbf{a}_1]_1 + \mathbf{Q}^1_2[\mathbf{a}_2]_2 + \cdots + \mathbf{Q}^1_2\mathbf{Q}^2_3\ldots\mathbf{Q}^{n-2}_{n-1}[\mathbf{a}_{n-1}]_{n-1} + \mathbf{Q}^1_2\ldots\mathbf{Q}^{n-1}_n[\mathbf{u}_n]_n + \mathbf{Q}^1_2\mathbf{Q}^{n-1}_n\mathbf{Q}^n_{n'}[\mathbf{s}_{b_n}]_{n'} \end{aligned} \tag{7}$$

$$\begin{aligned} [\bar{\mathbf{c}}_{p_n}]_1 &= \sum_{j=1}^{n-1}[\mathbf{a}_j]_1 + [\mathbf{u}_n]_1 + \rho_n[\mathbf{i}_{n'}]_1 + [\mathbf{s}_{p_n}]_1 \\ &= [\mathbf{a}_1]_1 + \mathbf{Q}^1_2[\mathbf{a}_2]_2 + \cdots + \mathbf{Q}^1_2\mathbf{Q}^2_3\ldots\mathbf{Q}^{n-2}_{n-1}[\mathbf{a}_{n-1}]_{n-1} + \mathbf{Q}^1_2\ldots\mathbf{Q}^{n-1}_n[\mathbf{u}_n]_n + \mathbf{Q}^1_2\ldots\mathbf{Q}^{n-1}_n\mathbf{Q}^n_{n'}\left(\rho_n[\mathbf{i}_{n'}]_{n'} + [\mathbf{s}_{p_n}]_{n'}\right) \end{aligned} \tag{8}$$

Finally, the angular velocities of the j^{th} actuator's barrel and piston assembly, measured with respect to ground and expressed in frame $X_1Y_1Z_1$, can be computed as:

$$[\boldsymbol{\omega}_{b_j}]_1 = [\boldsymbol{\omega}_{p_j}]_1 = \begin{bmatrix} 0 \\ 0 \\ \dot{\gamma}_j \end{bmatrix} \quad (j = 0,1) \qquad [\boldsymbol{\omega}_{b_j}]_1 = [\boldsymbol{\omega}_{p_j}]_1 = [\boldsymbol{\omega}_{l_{j-1}}]_1 + \mathbf{Q}^1_2\ldots\mathbf{Q}^{j-1}_j \begin{bmatrix} 0 \\ 0 \\ \dot{\gamma}_j \end{bmatrix} \quad (j = 2,3,4) \tag{9}$$

4. DYNAMIC MODELING

To develop the dynamic model for the rockbreaker, the Lagrange-Euler method was used with the joint angles θ_i defined as the generalized coordinates. The Lagrange-Euler formulation can be described as:

$$\frac{d}{dt}\frac{\partial T}{\partial \dot{\theta}_i} - \frac{\partial T}{\partial \theta_i} + \frac{\partial U}{\partial \theta_i} = \tau_i, \;\; i = 1,2,3,4 \tag{10}$$

where T and U represent the total kinetic energy and potential energy, respectively, stored within the system's rigid bodies. The kinetic and potential energies can be decomposed into contributions from the links (l), actuator barrels (b) and actuator pistons (p) such that $T = T_l + T_b + T_p$ and $U = U_l + U_b + U_p$ with:

$$T_l = \frac{1}{2}m_{l_i}\dot{\bar{\mathbf{c}}}^T_{l_i}\dot{\bar{\mathbf{c}}}_{l_i} + \frac{1}{2}\boldsymbol{\omega}^T_{l_i}\mathbf{Q}^1_{i+1}\bar{\mathbf{I}}_{l_i}\left(\mathbf{Q}^1_{i+1}\right)^T\boldsymbol{\omega}_{l_i}, \quad U_l = -g\mathbf{e}^T_g\left(\sum_{i=1}^{4} m_{l_i}\bar{\mathbf{c}}_{l_i}\right), \quad i = 1,2,3,4 \tag{11}$$

$$T_b = \frac{1}{2} m_{b_j} \dot{\bar{\mathbf{c}}}_{b_j}^T \dot{\bar{\mathbf{c}}}_{b_j} + \frac{1}{2} \boldsymbol{\omega}_{b_j}^T \mathbf{Q}_{j'}^1 \bar{\mathbf{I}}_{b_j} \left(\mathbf{Q}_{j'}^1\right)^T \boldsymbol{\omega}_{b_j}, \quad U_b = -g \mathbf{e}_g^T \left(\sum_{j=0}^{4} m_{b_j} \bar{\mathbf{c}}_{b_j} \right), \quad j = 0,1,...,4 \tag{12}$$

$$T_p = \frac{1}{2} m_{p_j} \dot{\bar{\mathbf{c}}}_{p_j}^T \dot{\bar{\mathbf{c}}}_{p_j} + \frac{1}{2} \boldsymbol{\omega}_{p_j}^T \mathbf{Q}_{j'}^1 \bar{\mathbf{I}}_{p_j} \left(\mathbf{Q}_{j'}^1\right)^T \boldsymbol{\omega}_{p_j}, \quad U_p = -g \mathbf{e}_g^T \left(\sum_{j=0}^{4} m_{p_j} \bar{\mathbf{c}}_{p_j} \right), \quad j = 0,1,...,4 \tag{13}$$

In these equations, m_{l_i}, m_{b_j} and m_{p_j} represent the masses of the i^{th} link, j^{th} actuator barrel and j^{th} actuator piston assembly, respectively. Meanwhile, $\dot{\bar{\mathbf{c}}}_{l_i}$, $\dot{\bar{\mathbf{c}}}_{b_j}$ and $\dot{\bar{\mathbf{c}}}_{p_j}$ represent the absolute velocities of each rigid body's centre of mass. The inertia matrix of the i^{th} link measured in a frame parallel to the $X_{i+1}Y_{i+1}Z_{i+1}$ frame with origin at C_{l_i} is represented as $\bar{\mathbf{I}}_{l_i}$. Similarly, the inertia matrices of the j^{th} actuator barrel and piston assembly measured in reference frames parallel to the $Y_j'Y_j'Z_j'$ frame with origins at C_{b_j} and C_{p_j}, respectively, are represented as $\bar{\mathbf{I}}_{b_j}$ and $\bar{\mathbf{I}}_{p_j}$. Finally, $g = 9.80655$ m/s^2 is the gravitational acceleration and $\mathbf{e}_g$ is a unit vector parallel to the gravitational field (i.e., $[\mathbf{e}_g]_1 = [0,0,-1]^T$). Using the Lagrange-Euler method, the complete dynamic model can then be obtained as:

$$\boldsymbol{\tau} = \mathbf{M}(\boldsymbol{\theta})\ddot{\boldsymbol{\theta}} + \mathbf{v}(\boldsymbol{\theta}, \dot{\boldsymbol{\theta}}) + \mathbf{g}(\boldsymbol{\theta}) \tag{14}$$

where the generalized inertia matrix $\mathbf{M}$, the vector of the Coriolis and centrifugal effects $\mathbf{v}$ and the vector of gravitational effects $\mathbf{g}$ can be divided into two parts: one due to contributions from the main links of the rockbreaker (labeled *link*) and the other due to contributions from the hydraulic actuators (both barrels and piston assemblies, labeled *act*) such that $\mathbf{M}(\boldsymbol{\theta}) = \mathbf{M}_{link}(\boldsymbol{\theta}) + \mathbf{M}_{act}(\boldsymbol{\theta})$, $\mathbf{v}(\boldsymbol{\theta}, \dot{\boldsymbol{\theta}}) = \mathbf{v}_{link}(\boldsymbol{\theta}, \dot{\boldsymbol{\theta}}) + \mathbf{v}_{act}(\boldsymbol{\theta}, \dot{\boldsymbol{\theta}})$, and $\mathbf{g}(\boldsymbol{\theta}) = \mathbf{g}_{link}(\boldsymbol{\theta}) + \mathbf{g}_{act}(\boldsymbol{\theta})$. Moreover, $\boldsymbol{\tau} = [\tau_1, \tau_2, \tau_3, \tau_4]^T$ is the vector of joint torques where τ_i is the torque that is applied indirectly to revolute joint R_i by the hydraulic actuators.

To develop the dynamic model in the form presented in Eq.(14), symbolic math software (Maxima) was used. Detailed expressions for the generalized inertia matrix ($\mathbf{M}$), Coriolis and centrifugal effects term ($\mathbf{v}$) and gravitational effects term ($\mathbf{g}$) are not presented in this article due to space limitations. Validation of the analytical model was done by comparing the results with a model developed using the Simscape Multibody toolbox in MATLAB/SIMULINK®. Computed joint torques from both models were found to match to a precision of 1×10^{-6} N·m, which corresponds to the precision of the model parameters used in the simulations. In order to improve the computational efficiency and reduce model complexity, simplified versions of the dynamic model are introduced as follows:

$$\boldsymbol{\tau}_1 = \mathbf{M}_{link}(\boldsymbol{\theta})\ddot{\boldsymbol{\theta}} + \mathbf{v}_{link}(\boldsymbol{\theta}, \dot{\boldsymbol{\theta}}) + \mathbf{g}(\boldsymbol{\theta}) \tag{15}$$

$$\boldsymbol{\tau}_2 = \mathbf{M}_{link}(\boldsymbol{\theta})\ddot{\boldsymbol{\theta}} + \mathbf{v}_{link}(\boldsymbol{\theta}, \dot{\boldsymbol{\theta}}) + \mathbf{g}_{link}(\boldsymbol{\theta}) \tag{16}$$

$$\boldsymbol{\tau}_3 = \mathbf{M}_{link}(\boldsymbol{\theta})\ddot{\boldsymbol{\theta}} + \mathbf{g}(\boldsymbol{\theta}) \tag{17}$$

In all cases, the contributions of the hydraulic actuators to $\mathbf{M}(\boldsymbol{\theta})$ and $\mathbf{v}(\boldsymbol{\theta}, \dot{\boldsymbol{\theta}})$ have been neglected although their contribution to $\mathbf{g}(\boldsymbol{\theta})$ has been maintained in the models described by Eqs. (20) and (22). These simplified models will be compared to the full dynamic model in terms of joint torques corresponding to prescribed rockbreaker trajectories. The objective is to identify a dynamic model of reduced complexity that would still generate joint torques sufficiently close to those obtained from the full model. The incorporation of a model-based component with a high accuracy into the control system will reduce the feedback control gains and will help to maintain a reasonable stability region around the equilibrium point [11]. It is estimated that joint torque errors less than approximately $\pm 10\%$ between a simplified dynamic model and the full model described by Eq. (14) would contribute to meeting this objective. However, this would need to be verified through implementation of a model-based controller on the actual rockbreaker.

5. SIMULATION RESULTS

The use of the dynamic model in an adaptive control scheme requires it to be expressed in parameterized form, which would be a complex task if the complete dynamic model were used. For this reason, simulations using the simplified dynamic models that were introduced in Eqs. (15) – (17) are run and the resulting joint torques errors compared to those obtained with the full dynamic model are analyzed. The goal is to identify a simplified dynamic model whose deviation from the full model is small enough to allow a suitable automated system performance through the use of a nonlinear dynamic model-based controller.

The simplified dynamic models are compared to the full dynamic model through the resulting joint torques (i.e., the torques applied indirectly to joints R_i by the hydraulic actuators). On one hand, the absolute joint torque error $\Delta\tau_{k,i}$ at the i^{th} joint will be computed as $\Delta\tau_{k,i} = |\tau_{k,i} - \tau_i|$ where τ_i is the torque obtained from the full dynamic model (from Eq. (14)) and $\tau_{k,i}$ ($k = 1,2,3$) is the one obtained from the k^{th} simplified dynamic model (Eqs. (15) – (17)). On the other hand, the relative joint torque error, defined as $\varepsilon_{k,i} = (\Delta\tau_{k,i}/\tau_i) \cdot 100\ (\%)$ will also be computed and analyzed over the simulated trajectories. The relative joint torque error is useful since it provides some perspective of the scale of the discrepancies between the different dynamic models. However, in some instances, the relative error becomes very large due to the fact that the actual joint torques (i.e., τ_i) are very small or equal to zero. In these cases, the absolute joint torque error, compared to the magnitude of the corresponding joint torques obtained from the full dynamic model, give a better indication of a simplified dynamic model's adequacy.

Simulations are based on predefined trajectories obtained with a trajectory planning algorithm. The algorithm that is used to generate the trajectories was developed for an actual rockbreaker system. Although the algorithm will not be described in detail here, it is important to note that it leads to trajectories meeting the following criteria:

- The flow rates to the hydraulic actuators do not exceed the allowable flow rates through the valves.
- The overall sum of flow rates to the hydraulic actuators does not exceed the hydraulic pump's maximum flow rate.
- Trajectories ensure smooth ramp-up and ramp-down of joint velocities.
- Trajectories ensure that at least one hydraulic actuator is operating at its maximum available flow rate at all times (to allow for the fastest motion possible).
- Trajectories maintain the breaker at an orientation as close as possible to vertical at all times (i.e. $\phi = 270$ degrees). Note that this is an operational requirement for the targeted application.
- Trajectories respect the mechanical limits of all joints.

Parameter values used in all simulations were taken from an actual rockbreaker and are provided in Appendix A. The following two trajectories, referred to as trajectory 1 and trajectory 2, were used to compare the simplified dynamic models to the full model:

- **Trajectory 1:** The tip of the breaker (i.e., point P) is displaced from $\mathbf{p}_{I_1} = [6.50,\ -2.50,\ -0.50]^T$ m to $\mathbf{p}_{F_1} = [2.55,\ 2.50,\ -0.50]^T$ m while its orientation changes from $\phi_{I_1} = 288$ degrees to $\phi_{F_1} = 270$ degrees. This is a motion where the breaker moves between diagonally-opposed corner openings of the grizzly within a horizontal plane located above the latter.
- **Trajectory 2:** The tip of the breaker (i.e., point P) is displaced from $\mathbf{p}_{I_2} = [4.50,\ 0.00,\ -0.50]^T$ m to $\mathbf{p}_{F_2} = [0.65,\ 4.95,\ 0.00]^T$ m while its orientation changes from $\phi_{I_2} = 270$ degrees to $\phi_{F_2} = 270$ degrees. This is a motion where the breaker moves from a central location above the grizzly to an arbitrary home position for the rockbreaker where it is parked when not in use.

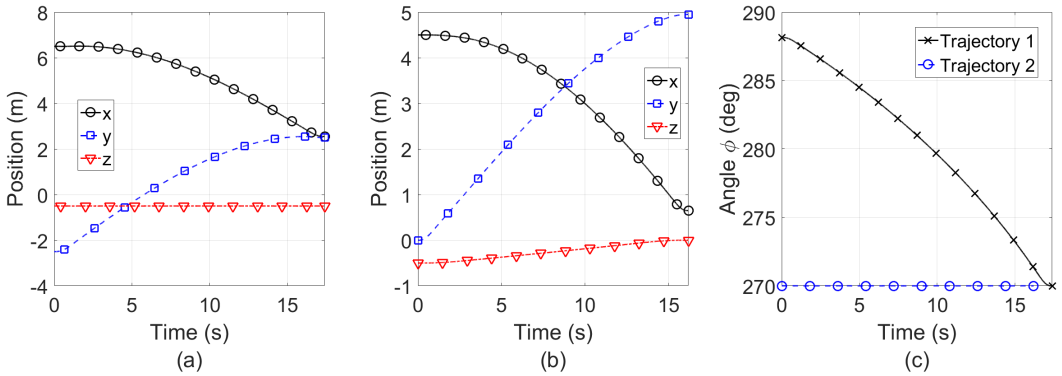

Fig. 3. Cartesian trajectories of rockbreaker used for dynamic simulations: (a) elements of position **p** for trajectory 1, (b) elements of position **p** for trajectory 2 and (c) orientation ϕ for trajectories 1 and 2.

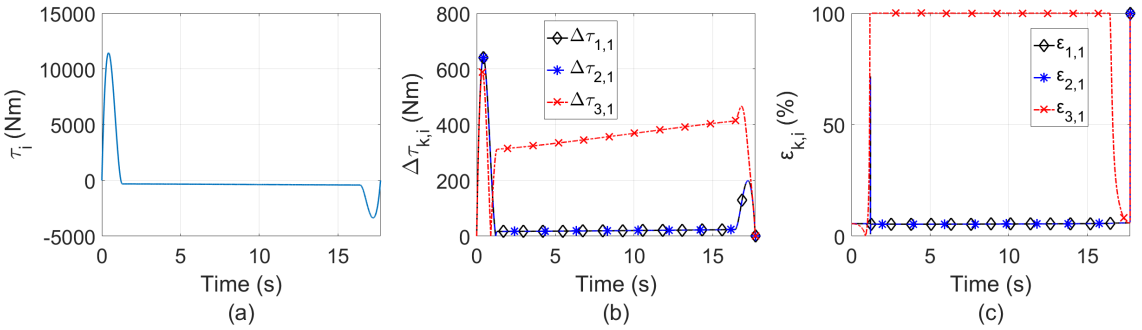

Fig. 4. Simulation results of torque at R_1 for trajectory 1: (a) computed joint torque using Eq. (14), (b) absolute joint torque errors and (c) relative joint torque errors using Eqs. (15) – (17).

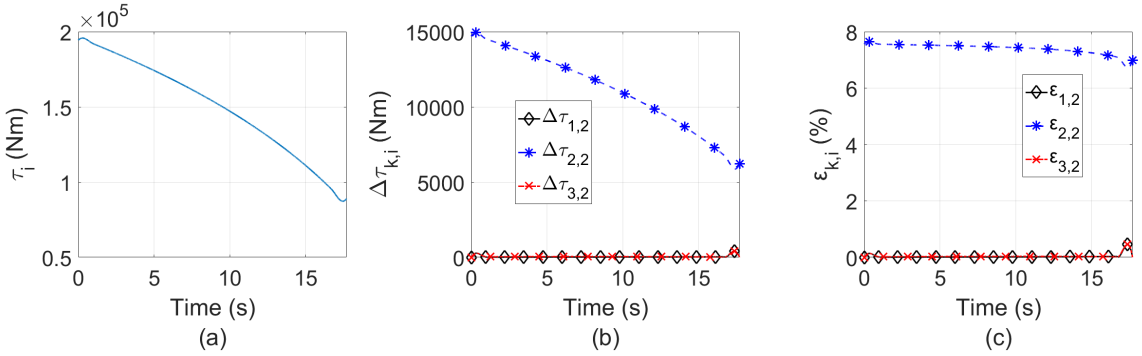

Fig. 5. Simulation results of torque at R_2 for trajectory 1: (a) computed joint torque using Eq. (14), (b) absolute joint torque errors and (c) relative joint torque errors using Eqs. (15) – (17).

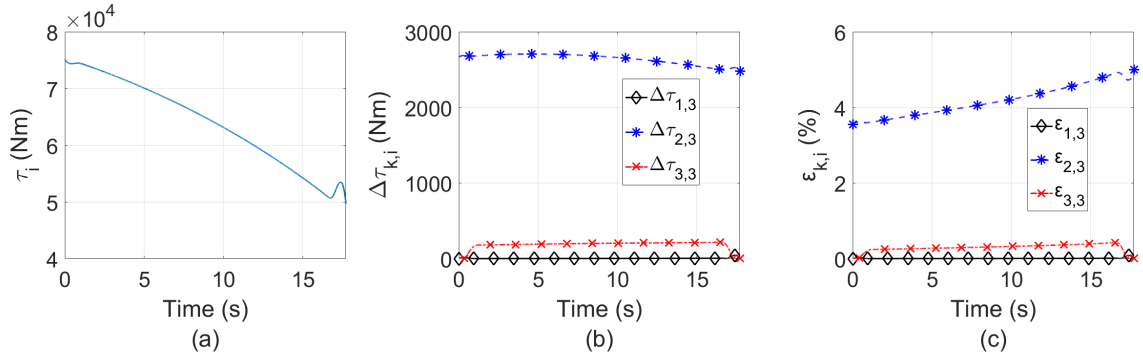

Fig. 6. Simulation results of torque at R_3 for trajectory 1: (a) computed joint torque using Eq. (14), (b) absolute joint torque errors and (c) relative joint torque errors using Eqs. (15) – (17).

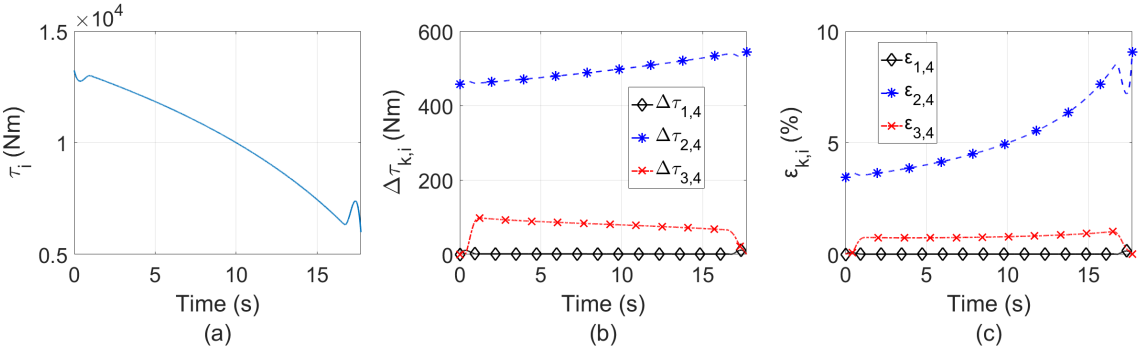

Fig. 7. Simulation results of torque at R_4 for trajectory 1: (a) computed joint torque using Eq. (14), (b) absolute joint torque errors and (c) relative joint torque errors using Eqs. (15) – (17).

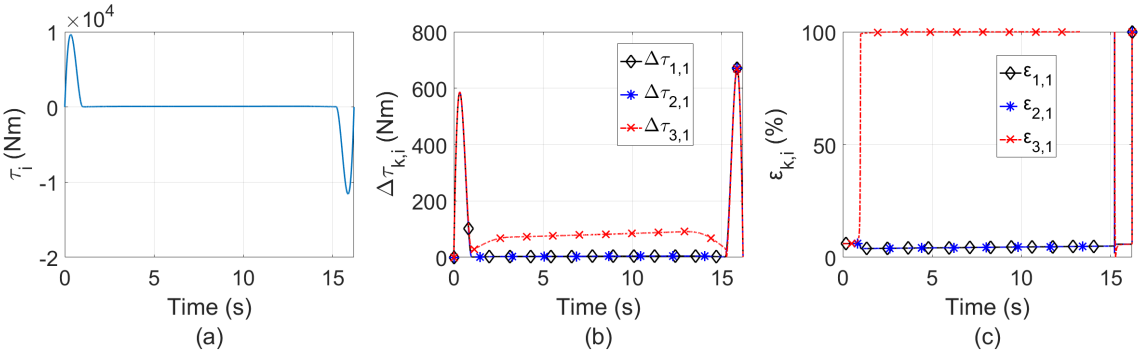

Fig. 8. Simulation results of torque at R_1 for trajectory 2: (a) computed joint torque using Eq. (14), (b) absolute joint torque errors and (c) relative joint torque errors using Eqs. (15) – (17).

The simulation results for trajectory 1 in terms of the full dynamic model's computed joint torque τ_i as well as the absolute and relative joint torque errors can be seen in Figs. 4 to 7. It can be observed that the best approximation of the full dynamic model is represented by $\boldsymbol{\tau}_1$. Its proximity to the full dynamic model suggests that the $\mathbf{M}_{act}\ddot{\boldsymbol{\theta}}$ and $\mathbf{v}_{act}$ terms have minimal impact on the system's dynamics. However, this model remains highly complex due to the $\mathbf{v}_{link}$ term and is therefore less than desirable for its implementation in an adaptive control scheme. Furthermore, it may be observed in Fig. 4 (b) and (c) that $\Delta\tau_{1,1} = \Delta\tau_{2,1}$ and $\varepsilon_{1,1} = \varepsilon_{2,1}$. This may be explained by the fact that the differentiating term between both models is the gravitational effects term which has no effect on the R_1 joint torques. Looking at the plots of $\varepsilon_{1,i}$ and $\varepsilon_{2,i}$ in Figs. 5 to 7, the considerable influence of the gravitational effect of the actuators $\mathbf{g}_{act}$ on the joint torques, accounting for as much as 8% of the joint torques computed from the full dynamic model, suggests that $\boldsymbol{\tau}_2$ is not a suitable simplified dynamic model. Lastly, as can be observed in Fig. 4(c), $\varepsilon_{3,1}$ reaches 100% in the central portion of the simulated trajectory (where $\ddot{\theta}_i = 0$) due to the complete omission of the $\mathbf{v}$ term in $\boldsymbol{\tau}_3$ and the fact that $\mathbf{g}$ has no bearing on the swing joint at R_1. However, the relative errors of $\boldsymbol{\tau}_3$ for the subsequent joints ($\varepsilon_{3,2}$, $\varepsilon_{3,3}$ and $\varepsilon_{3,4}$ as seen in Figs. 5 to 7) do not exceed 1%.

The simulation results for trajectory 2 are shown in Figs. 8 to 11. Many of the observations made for trajectory 1 also apply to the simulation results of trajectory 2. It can be observed from Fig. 9(c) to Fig. 11(c) that the relative error $\varepsilon_{2,i}$ is quite considerable and even reaches approximately 10% at times, further validating the claim that the gravitational effects due to the hydraulic actuators are considerable and should not be ignored as was the case in [4–8]. Finally, in the case of trajectory 2, it may be observed that $\varepsilon_{3,2}$, $\varepsilon_{3,3}$ and $\varepsilon_{3,4}$ always remain less than 2%.

From the results obtained from both trajectories 1 and 2, the simplified model $\boldsymbol{\tau}_3$ appears to be an acceptable alternative to the full dynamic model for use in real world applications. Although the model for $\boldsymbol{\tau}_3$ may

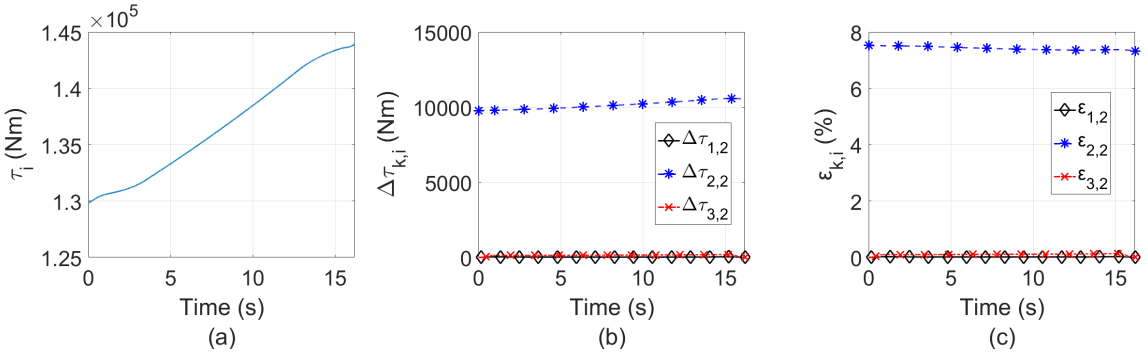

Fig. 9. Simulation results of torque at R_2 for trajectory 2: (a) computed joint torque using Eq. (14), (b) absolute joint torque errors and (c) relative joint torque errors using Eqs. (15) – (17).

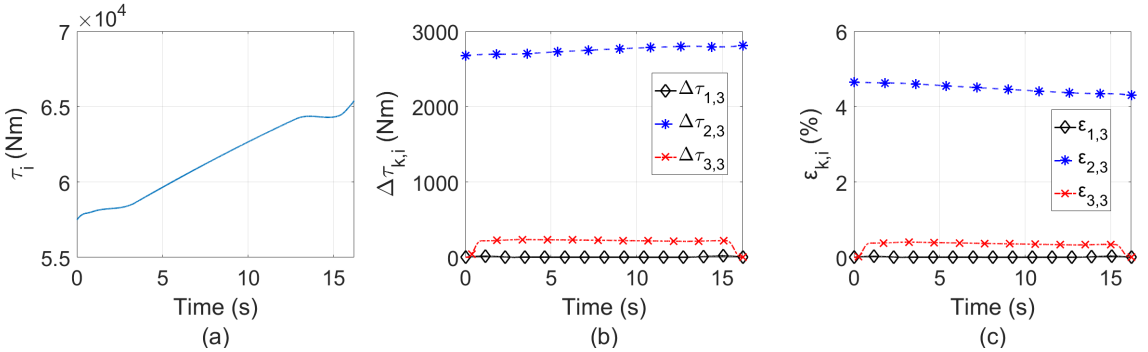

Fig. 10. Simulation results of torque at R_3 for trajectory 2: (a) computed joint torque using Eq. (14), (b) absolute joint torque errors and (c) relative joint torque errors using Eqs. (15) – (17).

not seem ideal for the torques at the swing joint (i.e., τ_1), it should be noted that the absolute error $\Delta\tau_{3,1}$, which reaches its maximum values during the velocity ramp-up and ramp-down portions of the trajectories (as seen in Fig. 4(b) and Fig. 8(b)), remains relatively small in magnitude with respect to the actual torques applied to this joint during those motions (as seen in Fig. 4(a) and Fig. 8(a)). Furthermore, it is believed that these errors could be mitigated with the addition to $\boldsymbol{\tau}_3$ of a simplified term replacing the currently omitted $\mathbf{v}_{link}$ term. The parameters within such a simplified term would need to be identified as part of the adaptive control algorithm implementation.

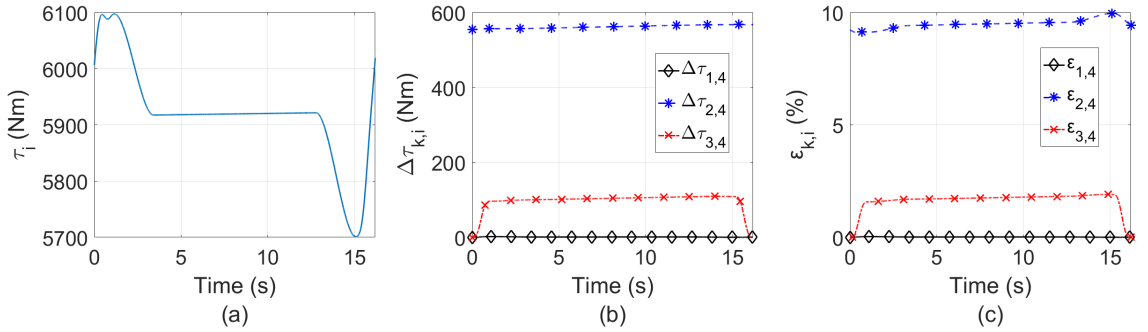

Fig. 11. Simulation results of torque at R_4 for trajectory 2: (a) computed joint torque using Eq. (14), (b) absolute joint torque errors and (c) relative joint torque errors using Eqs. (15) – (17).

6. CONCLUSION

This paper has investigated potential simplifications to the dynamic model of a hydraulic rockbreaker with the goal of identifying a suitable model for use in a model-based controller. It was found that the model proposed in Eq. (17), where the vector of Coriolis and centrifugal effects ($\mathbf{v}$) is entirely neglected and where the hydraulic actuators are only considered in static terms (i.e., their contribution to $\mathbf{g}$) is an attractive alternative to the full dynamic model. It allows for the computation of joint torques τ_2, τ_3 and τ_4 (i.e., joint torques which contribute to supporting the weight of the rockbreaker's parts) with an error of less than 2% measured relative to the torques obtained from the full dynamic model. The corresponding estimation of τ_1, however, is less accurate owing to the fact that it is not influenced by gravity. The investigation of how this might be addressed through the inclusion of an additional term to compensate for the exclusion of $\mathbf{v}$ without replicating its complexity is left to future work. The dynamic model described in this paper did not consider viscous or Coulomb friction at the revolute and prismatic joints. It is believed, however, that friction has a non-negligible effect on the system's dynamics. Also left to future work is the inclusion of friction models with coefficients needing to be identified through an adaptive control scheme.

REFERENCES

1. Sciavicco, L. and Siciliano, B. *Modelling and Control of Robot Manipulators*. 2 ed.. Springer, 2000.
2. Slotine, J.J.E. and Li, W. "On the adaptive control of robot manipulators." *The International Journal of Robotics Research*, Vol. 6, No. 3, pp. 49–59, 1987.
3. Craig, J.J., Hsu, P. and Sastry, S.S. "Adaptive control of mechanical manipulators." *The International Journal of Robotics Research*, Vol. 6, No. 2, pp. 16–28, 1987.
4. Vaha, P.K. and Skibniewski, M.J. "Dynamic model of excavator." *Journal of Aerospace Engineering*, Vol. 6, No. 2, pp. 148–158, 1993.
5. Koivo, A.J., Thoma, M., Kocaoglan, E. and Andrade-Cetto, J. "Modeling and control of excavator dynamics during digging operation." *Journal of Aerospace Engineering*, Vol. 9, No. 1, pp. 10–18, 1996.
6. Frimpong, S., Hu, Y. and Inyang, H. "Dynamic modeling of hydraulic shovel excavators for geomaterials." *Internation Journal of Geomechanics*, Vol. 8, No. 1, pp. 20–29, 2008.
7. Salinic, S., Boskovic, G. and Nikolic, M. "Dynamic modelling of hydraulic excavator motion using Kane's equations." *Automation in Construction*, Vol. 44, No. 1, pp. 56–62, 2014.
8. Patel, B.P. and Prajapati, J. "Dynamics of mini hydraulic backhoe excavator:a lagrange-euler (l-e) approach." *International Journal of Mechanical, Aerospace, Industrial, Mechatronic and Manufacturing Engineering*, Vol. 8, No. 1, pp. 195–204, 2014.
9. Chang, P.H. and Lee, S.L. "A straight-line moition tracking control of hydraulic excavator system." *Mechatronics*, Vol. 12, No. 1, pp. 119–138, 2002.
10. Angeles, J. *Fundamentals of robotic mechanical systems: Theory, methods, and algorithms*. Third ed.. Springer Science+Business Media, 2007.
11. Kokotovic, P. and Marino, R. "On vanishing stability regions in nonlinear systems with high-gain feedback." *IEEE Transactions on Automatic Control*, Vol. 31, No. 10, pp. 967 – 970, 1986.

APPENDIX A

Table 1. Denavit-Hartenburg parameter values.

i	a_i (m)	b_i (m)	α_i (deg.)
1	0.349	1.049	90
2	3.397	0.000	0
3	2.642	0.000	0
4	2.219	0.000	0

Table 2. Masses of links, actuator barrels and piston assemblies.

$$m_{l_1} = 1029.59 \text{ kg}, \quad m_{l_2} = 1313.70 \text{ kg}, \quad m_{l_3} = 975.41 \text{ kg}, \quad m_{l_4} = 2082.98 \text{ kg}$$
$$m_{b_0} = m_{b_1} = 51.61 \text{ kg}, \quad m_{b_2} = m_{b_3} = m_{b_4} = 134.96 \text{ kg}, \quad m_{p_0} = m_{p_1} = 33.52 \text{ kg}, \quad m_{p_2} = m_{p_3} = m_{p_4} = 84.99 \text{ kg}$$

Table 3. Positions of links' centres of mass.

$$[\mathbf{s}_{l_1}]_2 = \begin{bmatrix} -0.044 \\ -0.432 \\ -0.006 \end{bmatrix} \text{ m}, \quad [\mathbf{s}_{l_2}]_3 = \begin{bmatrix} -1.618 \\ 0.044 \\ -0.001 \end{bmatrix} \text{ m}, \quad [\mathbf{s}_{l_3}]_4 = \begin{bmatrix} -1.865 \\ 0.082 \\ -0.001 \end{bmatrix} \text{ m}, \quad [\mathbf{s}_{l_4}]_5 = \begin{bmatrix} -1.001 \\ 0.126 \\ 0.002 \end{bmatrix} \text{ m}$$

Table 4. Positions of actuator barrels' centres of mass.

$$[\mathbf{s}_{b_0}]'_0 = [\mathbf{s}_{b_1}]'_1 = \begin{bmatrix} 0.396 \\ 0.000 \\ 0.000 \end{bmatrix} \text{ m}, \quad [\mathbf{s}_{b_2}]'_2 = \begin{bmatrix} 0.703 \\ -0.005 \\ 0.001 \end{bmatrix} \text{ m}, \quad [\mathbf{s}_{b_3}]'_3 = [\mathbf{s}_{b_4}]'_4 = \begin{bmatrix} 0.703 \\ 0.005 \\ -0.001 \end{bmatrix} \text{ m}$$

Table 5. Positions of actuator piston assemblies' centres of mass.

$$[\mathbf{s}_{p_0}]'_0 = [\mathbf{s}_{p_1}]'_1 = \begin{bmatrix} -0.394 \\ 0.000 \\ 0.000 \end{bmatrix} \text{ m}, \quad [\mathbf{s}_{p_2}]'_2 = [\mathbf{s}_{p_3}]'_3 = [\mathbf{s}_{p_4}]'_4 = \begin{bmatrix} -0.783 \\ 0.000 \\ 0.000 \end{bmatrix} \text{ m}$$

Table 6. Positions of A_j nodes with respect to R_i nodes.

$$[\mathbf{u}_0]_1 = \begin{bmatrix} -1.163 \\ -0.375 \\ 0.419 \end{bmatrix} \text{ m}, \quad [\mathbf{u}_1]_1 = \begin{bmatrix} -1.163 \\ 0.375 \\ 0.419 \end{bmatrix} \text{ m}, \quad [\mathbf{u}_2]_2 = \begin{bmatrix} 0.318 \\ -0.706 \\ 0 \end{bmatrix} \text{ m}, \quad [\mathbf{u}_3]_3 = \begin{bmatrix} -2.254 \\ 0.434 \\ 0 \end{bmatrix} \text{ m}, \quad [\mathbf{u}_4]_4 = \begin{bmatrix} -2.316 \\ 0.405 \\ 0 \end{bmatrix} \text{ m}$$

Table 7. Inertial matrices of links (kg·m^2).

$$[\mathbf{I}_{l_1}]_2 = \begin{bmatrix} 158.98 & 0.94 & -0.63 \\ 0.94 & 65.74 & -1.79 \\ -0.63 & -1.79 & 164.75 \end{bmatrix}, \qquad [\mathbf{I}_{l_2}]_3 = \begin{bmatrix} 50.53 & 622.48 & -1.66 \\ 622.48 & 1079.78 & 0.03 \\ -1.66 & 0.03 & 1468.53 \end{bmatrix}$$

$$[\mathbf{I}_{l_3}]_4 = \begin{bmatrix} 797.82 & -489.64 & 0.66 \\ -489.64 & 347.07 & -0.11 \\ 0.66 & -0.11 & 1117.27 \end{bmatrix}, \quad [\mathbf{I}_{l_4}]_5 = \begin{bmatrix} 107.94 & 203.52 & -3.73 \\ 203.52 & 1355.62 & 0.68 \\ -3.73 & 0.68 & 1397.74 \end{bmatrix}$$

Table 8. Inertial matrices of actuator barrels (kg·m^2).

$$[\mathbf{I}_{b_0}]_{0'} = [\mathbf{I}_{b_1}]_{1'} = \begin{bmatrix} 0.22 & 0.00 & 0.00 \\ 0.00 & 3.70 & 0.00 \\ 0.00 & 0.00 & 3.71 \end{bmatrix}, \quad [\mathbf{I}_{b_2}]_{2'} = \begin{bmatrix} 0.91 & 0.18 & -0.07 \\ 0.18 & 31.90 & -0.02 \\ -0.07 & -0.02 & 31.99 \end{bmatrix}, \quad [\mathbf{I}_{b_3}]_{3'} = [\mathbf{I}_{b_4}]_{4'} = \begin{bmatrix} 0.91 & -0.18 & 0.07 \\ -0.18 & 31.90 & 0.02 \\ 0.07 & 0.02 & 31.99 \end{bmatrix}$$

Table 9. Inertial matrices of actuator piston assemblies (kg·m^2).

$$[\mathbf{I}_{p_0}]_{0'} = [\mathbf{I}_{p_1}]_{1'} = \begin{bmatrix} 0.035 & 0.00 & 0.00 \\ 0.00 & 2.49 & 0.00 \\ 0.00 & 0.00 & 2.50 \end{bmatrix}, \quad [\mathbf{I}_{p_2}]_{2'} = [\mathbf{I}_{p_3}]_{3'} = [\mathbf{I}_{p_4}]_{4'} = \begin{bmatrix} 0.11 & 0.00 & 0.00 \\ 0.00 & 18.72 & 0.00 \\ 0.00 & 0.00 & 18.73 \end{bmatrix}$$